JOURNAL OF APPLIED PHYSICS **115**, 233708 (2014)

Fermi level stabilization and band edge energies in $Cd_xZn_{1-x}O$ alloys

Douglas M. Detert,[1,2] Kyle B. Tom,[1,2] Corsin Battaglia,[1,3] Jonathan D. Denlinger,[4] Sunnie H. N. Lim,[5] Ali Javey,[1,3] André Anders,[6] Oscar D. Dubon,[1,2] Kin M. Yu,[1] and Wladek Walukiewicz[1]

[1]*Materials Sciences Division, Lawrence Berkeley National Laboratory, Berkeley, California 94720, USA*
[2]*Department of Materials Science and Engineering, University of California, Berkeley, California 94720, USA*
[3]*Department of Electrical Engineering and Computer Sciences, University of California, Berkeley, California 94720, USA*
[4]*Advanced Light Source, Lawrence Berkeley National Laboratory, Berkeley, California 94720, USA*
[5]*Environmental Energy Technologies Division, Lawrence Berkeley National Laboratory, Berkeley, California 94720, USA*
[6]*Accelerator and Fusion Research Division, Lawrence Berkeley National Laboratory, Berkeley, California 94720, USA*

(Received 24 April 2014; accepted 10 June 2014; published online 18 June 2014)

We have measured the band edge energies of $Cd_xZn_{1-x}O$ thin films as a function of composition by three independent techniques: we determine the Fermi level stabilization energy by pinning the Fermi level with ion irradiation, measure the binding energy of valence band states and core levels by X-ray photoelectron spectroscopy, and probe shifts in the conduction band and valence band density of states using soft X-ray absorption and emission spectroscopy, respectively. The three techniques find consensus in explaining the origin of compositional trends in the optical-bandgap narrowing upon Cd incorporation in wurtzite ZnO and widening upon Zn incorporation in rocksalt CdO. The conduction band minimum is found to be stationary for both wurtzite and rocksalt alloys, and a significant upward rise of the valence band maximum accounts for the majority of these observed bandgap changes. Given these band alignments, alloy disorder scattering is found to play a negligible role in decreasing the electron mobility for all alloys. These band alignment details, combined with the unique optical and electrical properties of the two phase regimes, make CdZnO alloys attractive candidates for photoelectrochemical water splitting applications. [http://dx.doi.org/10.1063/1.4884683]

I. INTRODUCTION

Thin films of the CdO–ZnO pseudobinary alloy system have garnered attention in recent years for their potential optoelectronic use. The structural mismatch between the endpoint compounds, wurtzite (WZ)-ZnO and rocksalt (RS)-CdO, gives rise to two distinct phase regimes for $Cd_xZn_{1-x}O$ alloys, each with distinct optical and electrical properties: WZ-structured alloys have a direct optical bandgap that can be tuned over the visible range, and high-electron-mobility RS-structured alloys are attractive transparent conductors.[1–11]

In our previous work, we examined the basic properties of this alloy system over the entire composition range.[11] At low to moderate Cd content ($x < 0.69$), the films are predominantly WZ-structured and exhibit a direct energy gap and strong band edge photoluminescence that can be tuned from 3.3 eV (pure ZnO) to 1.7 eV. At high Cd content ($x > 0.69$), the films are RS-structured, have a high electron mobility ($\sim$90 $cm^2\ V^{-1}\ s^{-1}$), and exhibit an indirect bandgap (no detectable luminescence) and a larger direct gap that can be tuned from 2.3 eV (pure CdO) to 2.6 eV ($x = 0.75$).

In this work, we relate the changes in the optical bandgap to the independent movement of the conduction-band minimum (CBM) and valence-band maximum (VBM) across the composition range. The compositional shifts in the band-edge positions have previously been studied using first-principles calculations,[12,13] but to date there is little experimental evidence to confirm these electronic-structure calculations beyond one report of $Cd_xZn_{1-x}O$ alloys up to $x = 0.075$.[10] Here, we employ three different techniques—high energy ion irradiation, X-ray photoelectron spectroscopy (XPS), and soft X-ray absorption and emission spectroscopy (XAS/SXE)—to build a consistent picture of the band alignment as a function of Cd content for both the WZ and RS structure alloys. We compare the experimental results with existing theoretical calculations and briefly discuss the potential applications of the CdZnO materials system for solar power conversion.

II. FILM GROWTH

$Cd_xZn_{1-x}O$ thin films across the composition range were deposited by pulsed filtered cathodic arc deposition (PFCAD) on glass substrates at 300 °C. X-ray diffraction (XRD) reveals that the films are polycrystalline with an average grain size of 20 nm; WZ films are {0002} textured, while RS films exhibit preferred {002} and {111} orientations, for $0.69 < x < 1$ and pure CdO, respectively. The experimental details of the film growth and the results of the basic structural, optical, and electrical characterization of the samples examined in this work are summarized in our previous work.[11] The phase transition from the WZ to the RS crystal structure at $x = 0.69$ corresponds with a step-increase in both the bandgap E_g^o and the electron mobility.

III. FERMI LEVEL PINNING BY ION IRRADIATION

The charge state as well as the formation energy of native defects in semiconductors is dependent on the position of the Fermi level E_F with respect to a universal energy level, known as the Fermi level stabilization energy E_{FS}, located ~4.9 eV below the vacuum level in all semiconductors.[14,15] When intentionally generated via ion irradiation, these electrically active, amphoteric defects move E_F toward E_{FS}, eventually pinning it at that energy; E_F is unaffected by further irradiation. In the case of materials where E_{FS} is closer to the CBM, the pinned value of E_F relative to the CBM is determined by the saturated value of the free electron concentration

$$n = \frac{1}{3\pi^2}\int_0^\infty \frac{\exp\left(z - \frac{E_F}{k_BT}\right)}{\left[1+\exp\left(z-\frac{E_F}{k_BT}\right)\right]^2} k^3(z)dz, \qquad (1)$$

where $z = E_C/k_BT$, E_C is the energy relative to the CBM, and the wavevector k is found using the non-parabolic dispersion as derived from Kane's two-band $\boldsymbol{k}\cdot\boldsymbol{p}$ model,[16]

$$E(k) = \frac{\hbar^2k^2}{2m_0} - \frac{E_g}{2} + \left(\sqrt{\left(\frac{E_g}{2}\right)^2 + \frac{E_g\hbar^2k^2}{2m_e^*}}\right). \qquad (2)$$

The electron effective mass m_e^* is assumed to be dependent on the bandgap following Ref. 11. The electron affinity E_{EA}, by extension, can be determined as $E_{EA} = E_{FS} + E_F$. When combined with E_g, this technique also establishes the energy of the valence band at the Γ-point with respect to the vacuum level. This method has previously been used to establish the position of E_{FS} in (and therefore the natural band alignment among) a number of elemental and compound semiconductors,[15,17] including the endpoint binary compounds, CdO ($E_{EA} = 5.9$ eV)[18] and ZnO ($E_{EA} = 4.85$ eV),[19] investigated in this study.

Point defects were generated by irradiating films with 120 keV Ne^+ ions in fluence increments of 5×10^{12} cm^{-2}, reaching a final total fluence of 3×10^{13} cm^{-2}. The electron concentration and mobility at each damage fluence were measured by room temperature Hall effect using the van der Pauw method and a 0.6 T magnetic field. Note that the thicknesses of the films used in this study (100–200 nm) were smaller than the projected range of the Ne^+ ions, ensuring that defects were generated relatively uniformly in the films.

The electrical properties as a function of total ion fluence are presented in Figure 1 and summarized in Table I. The electron concentration (Figure 1(a)) of WZ samples with low Cd-content ($x < 0.29$) decreases from $n \sim 10^{19}$ cm^{-3} (as-grown) to $n \sim 10^{18}$ cm^{-3} at saturation (total fluence: 3×10^{13} cm^{-2}). By contrast, the concentration in the WZ sample with $x = 0.56$ does not change appreciably with increasing fluence, and that of the RS samples (dotted lines) increases from $n \sim 1–2\times10^{20}$ cm^{-3} to a final saturation value of $n \sim 3\times10^{20}$ cm^{-3}. The mobility (Figure 1(b)) of each sample decreases with increasing total irradiation dose due to increasing scattering events from the ionized native defects. The resistivity of the pure ZnO

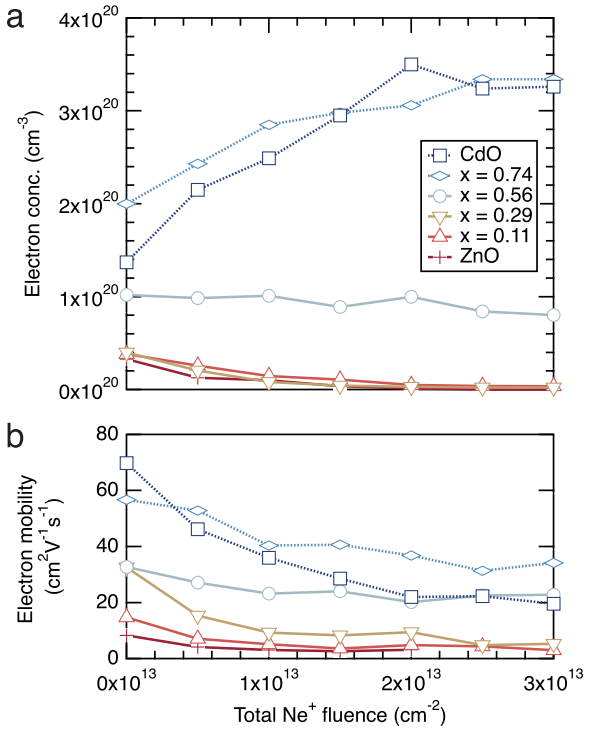

FIG. 1. Electrical properties of (120 keV Ne^+) ion-irradiated $Cd_xZn_{1-x}O$ films as a function of irradiation fluence, as measured by room temperature Hall effect. (a) Amphoteric point defects generated by ion irradiation move the Fermi level toward E_{FS}, eventually leading to a saturation in the free electron concentration when $E_F = E_{FS}$. (b) The mobility of each sample decreases with increasing total ion fluence.

sample was too large to provide accurate concentration and mobility values at total ion fluences above 2×10^{13} cm^{-2}. The last reliably measurable value of the electron concentration, 1.05×10^{18} cm^{-3} (with $\mu \sim 3.2$ cm^2 V^{-1} s^{-1}), agrees well with the saturation value observed in previous experiments.[19]

The compositional dependence of the films' electrical properties following irradiation is shown in Figure 2. As shown in Figure 2(a) and tabulated in Table I, the saturated electron concentrations for films with $x < 0.29$ are all close to 10^{18} cm^{-3}. The value of E_F with respect to the CBM (calculated using Eq. (1)) for these concentrations is close to zero, and we conclude that the CBM lies close to E_{FS} in this composition range (that is, $E_{EA} \approx 4.9$ eV). The saturation concentration of 8.0×10^{19} cm^{-3} for the highest Cd-content WZ film ($x = 0.56$) is significantly higher and indicates that the Fermi level is pinned ~350 meV above the CBM (with a corresponding increase in E_{EA}). For both of the RS samples, the saturated electron concentration indicates a high electron affinity with the CBM of each sample located ~0.8 eV below E_{FS}. The electron mobility of the samples is shown in Figure 2(b). It is somewhat surprising that maximum electron mobility is not observed at $x = 1$ (pure CdO) but rather in the alloy with $x = 0.74$ given that the saturation concentration is constant throughout the RS range. The reason for this behavior is unclear at present.

Within the framework of the amphoteric defect model, establishing the position of the CBM with respect to E_{FS} also yields valuable information regarding the extent of charge accumulation (or depletion) at surfaces. The surface Fermi level of

TABLE I. Summary of ion irradiation experiment to determine Fermi level stabilization energy and electron affinity in $Cd_xZn_{1-x}O$ films.

Cd content(x)	n_e (as-grown) (cm^{-3})	n_e (saturation) (cm^{-3})	μ_e (saturation) ($cm^2\ V^{-1}\ s^{-1}$)	E_f rel. to CBM (eV)	E_{EA} (eV)
0	$3.28^a \times 10^{19}$	$1.05^a \times 10^{18}$	3.2[a]	−0.013[a]	4.89
0.11	3.84×10^{19}	3.61×10^{18}	4.1	0.035	4.94
0.29	3.99×10^{19}	2.17×10^{18}	6.5	0.015	4.91
0.56	1.02×10^{20}	8.02×10^{19}	21.8	0.347	5.25
0.74	2.00×10^{20}	3.34×10^{20}	49.4	0.757	5.66
1	1.37×10^{20}	3.26×10^{20}	34.1	0.768	5.67

[a]The ZnO (x = 0) film became too resistive to measure above a total fluence of $2 \times 10^{13}\ cm^{-2}$.

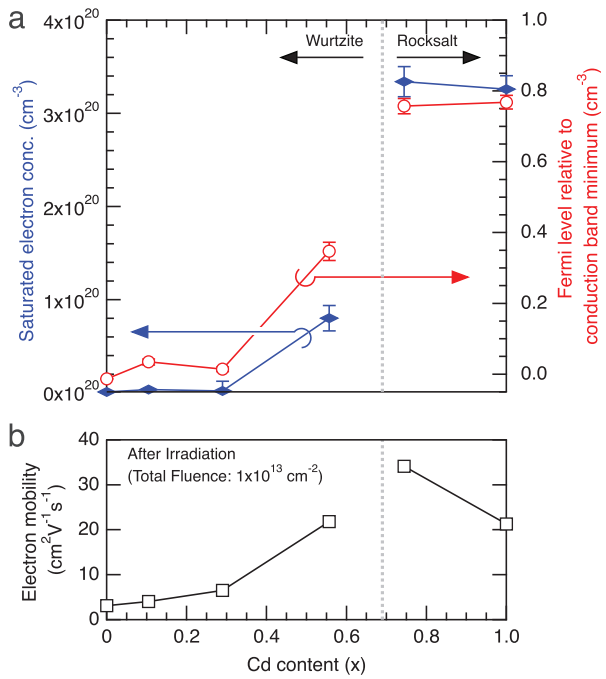

FIG. 2. Electrical properties of $Cd_xZn_{1-x}O$ films following irradiation as a function of Cd content. (a) The saturation value of the electron concentration, along with the corresponding shift in the Fermi level (following Eq. (1)), is constant for WZ films below x = 0.29, rises moderately near the phase transition point, and reaches higher values for the RS films. (b) The electron mobility of films following irradiation reaches a maximum for x = 0.74.

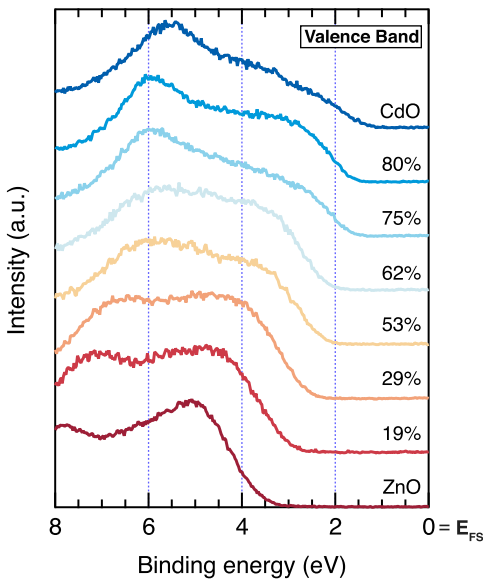

FIG. 3. XPS valence band spectra. A linear extrapolation of the band edge shows that the VBM shifts upward by ~1.4 eV across the WZ phase regime, moving to even lower binding energies for the RS alloys. The total shift in the VBM across the entire composition range is ~2.3 eV.

all samples (both as-grown and irradiated) can be assumed to be pinned at E_{FS}. Additional ion-induced defect generation in the bulk tends to align the bulk Fermi levels at E_{FS} attaining a flat band condition. For this reason, as the bulk Fermi level of all $Cd_xZn_{1-x}O$ samples is observed to lie close to or above the CBM, we expect downward band bending and electron accumulation at the surface and along internal extended defects of as-grown films. Similarly, the increase in E_{AE} from WZ to RS explains the rise in Hall concentration of as-grown films observed in Ref. 11 as native defects will have a greater tendency to act as donors as the CBM moves below E_{FS}.

IV. X-RAY PHOTOELECTRON SPECTROSCOPY

A separate set of $Cd_xZn_{1-x}O$ samples taken from the same growth series were examined by XPS in order to probe shifts in the valence-band maximum and core levels as a function of composition. XPS spectra were measured using a monochromated Al Kα X-ray source ($h\nu = 1486.6$ eV) with a Kratos Axis Ultra DLD hemispherical electron analyzer.

Valence band spectra of samples spanning the complete composition range are shown in Figure 3. The VBM for each sample was determined by taking a linear extrapolation of the valence band edge to zero intensity. There is a monotonic decrease in binding energy of the VBM over the entire composition range. Across the WZ phase regime, the binding energy of the VBM decreases from 3.3 eV (ZnO) to 2.2 eV (x = 0.53), whereas the binding energy of the VBM moves to even lower values (~1.6 eV) in the RS range.

In contrast to that of the WZ alloys, the onset of the valence band edge for the RS alloys is less abrupt. The shallower slope may indicate that the L-point VBM of the CdO endpoint established in previous studies is preserved with Zn incorporation.[20–22] As well, this conclusion is supported by the lack of band edge photoluminescence from the RS alloys.[11] While binding energies are plotted relative to the Fermi level of each sample, the surface sensitivity of XPS allows to reference the observed shifts to a common energy level because the Fermi level at the surface of each sample is inherently pinned at E_{FS}.

XPS also reveals chemical shifts in the oxygen 1s core-level energy across the composition range. As indicated in Figure 4, there are two components to the peak at the O 1s level: a high-binding-energy peak that is nearly static with Cd content and a lower binding-energy component that

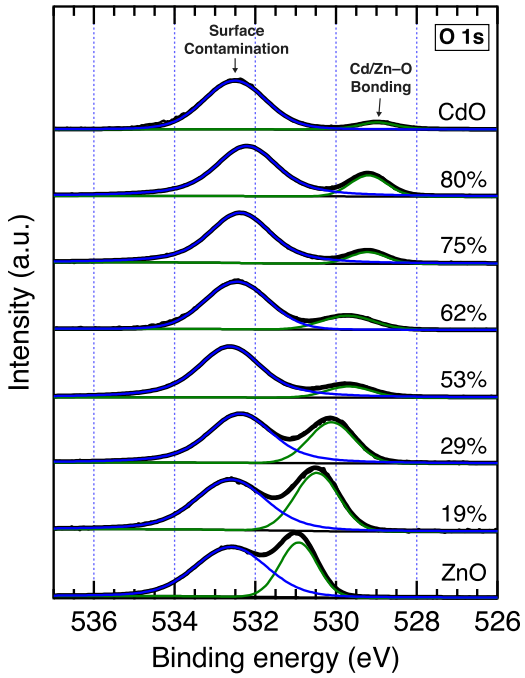

FIG. 4. Oxygen 1s core-level spectra for alloys across the composition range. The high binding-energy component can be attributed to surface contamination, following King *et al.*,[22] while the lower binding-energy feature arises from metal-oxygen bonding. XAS/SXE spectra recorded relative to the O 1s level (shown in Figure 5) must be corrected for the nearly 2 eV shift to lower binding energy with Cd content observed in this second peak.

exhibits a monotonic decrease in energy with increasing Cd content. These peaks were fitted with two Voigt lineshapes and a standard Shirley background. As shown by King *et al.* for the case of binary CdO and ZnO, the high-binding-energy feature arises from surface contamination, while the presence of the lower binding-energy peak is due to Cd-O and Zn-O bonding.[22] Over the entire composition range, the peak moves by nearly 2 eV, a shift that is consistent with that reported in Ref. 23. As described in Sec. V, it is critically important to account for such core-level shifts when performing X-ray absorption and emission spectroscopy.

V. SOFT X-RAY ABSORPTION AND EMISSION SPECTROSCOPIES

In order to independently and directly probe changes in the conduction and valence band edges as a function of composition, we have further analyzed our $Cd_xZn_{1-x}O$ films using XAS/SXE to measure the oxygen partial density of states in the conduction and valence bands, respectively. For each of the samples previously analyzed by XPS, we recorded oxygen K-edge absorption spectra and oxygen-resonance emission spectra at Beamline 8.0.1 of the Advanced Light Source at Lawrence Berkeley National Laboratory. The absorption spectra, measured by total fluorescence yield, were recorded with the sample oriented 45° relative to the direction of incidence; the emission spectra were recorded using 530 eV photon excitation. The SXE spectra were normalized such that the maximum intensity value of each was scaled to 1. The XAS spectra were first normalized to a common value far above threshold (556 eV) before the spectra were uniformly scaled to set the maximum intensity (of the CdO spectrum) to 1.

The intensity-normalized spectra are presented in Figure 5. Figure 5(b) provides a magnified scale to show changes in the absorption and emission edges with composition. These "uncorrected" spectra appear to suggest that the VBM, found by extrapolating each curve to the horizontal axis, is stationary with composition and that the narrowing of the gap with Cd content is caused by a nearly 2 eV decrease in the CBM energy. The energy scale of the spectra presented in the upper panels of Figures 5(a) and 5(b) references the incident and emitted photon energies, and thus its features are measured with respect to the O 1s core level. As demonstrated in the XPS measurements, however, the energy of this core level is not constant with alloy composition. As a result, the positions of the as-recorded, "uncorrected" absorption and emission edges do not represent energy shifts in the unfilled conduction band (XAS) and filled valence band (SXE) states on an absolute scale.

The compositional changes in the CBM and VBM can be assessed by shifting the XAS/SXE spectra by the change

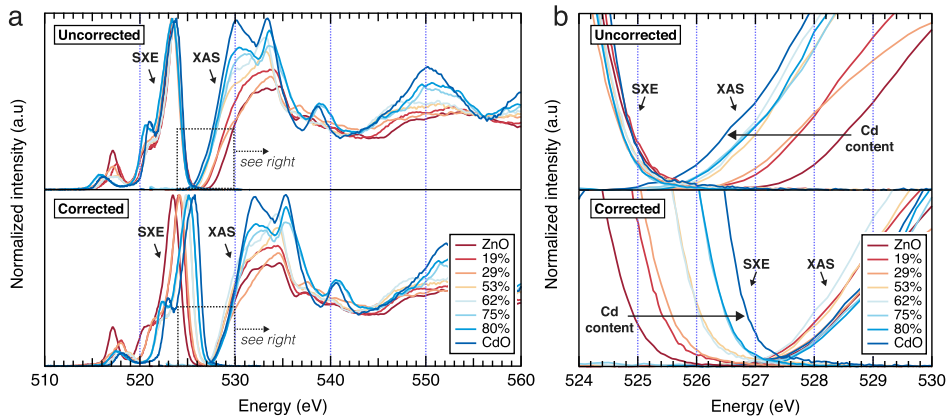

FIG. 5. Normalized soft X-ray absorption and emission spectra for samples across the composition range, uncorrected (top) and corrected (bottom) for chemical shifts in the O 1s core level position shown in Figure 4. The full normalized XAS/SXE spectra are shown in (a) while a magnified energy scale in (b) reveals shifts in the density of states near the VBM (SXE) and CBM (XAS). The band edge shifts with Cd content suggested by the uncorrected spectra (the downward movement of the CBM and a stationary VBM) are reversed when the movement of the core level position is taken into account. The corrected spectra reveal a rise in the VBM density of states and a relatively stationary CBM (XAS).

in its O 1s level, as measured by XPS, relative to that of ZnO. The corrected spectra, shown in the lower panels of Figures 5(a) and 5(b), reveal that with increasing Cd content there is a systematic rise in the emission edge, while the absorption edge remains relatively constant across the composition range. The 2 eV rise in the VBM observed by SXE is consistent with the VBM shift measured by XPS in Figure 3.

VI. BAND EDGE ENERGIES

A summary of the results from the three independent measurements of the conduction and valence band edge positions is presented in Figure 6. The irradiation and XPS results, as discussed previously, can be independently placed on an absolute energy scale, while the relative shifts in the band edges extrapolated from the XAS/SXE spectra are placed on the same absolute scale by matching the value of the VBM (SXE) and CBM (XAS) to the absolute values obtained from XPS and irradiation, respectively.

In two of the measurement techniques, the position of only one band edge is measured independently, but in both cases the energy of the other band can be inferred by including the intrinsic, direct bandgap E_g found by correcting the measured optical absorption edge for free carrier effects.[11] In this way, irradiation-induced Fermi-level pinning directly measures the CBM and indirectly yields the valence band at the Γ-point, as optical transitions are always direct. For direct-gap WZ alloys, the VBM is located at the Γ-point. For RS alloys, as is the case with CdO, however, the VBM is positioned at the L symmetry point and gives rise to an indirect bandgap. In the case of the RS alloys, therefore, the

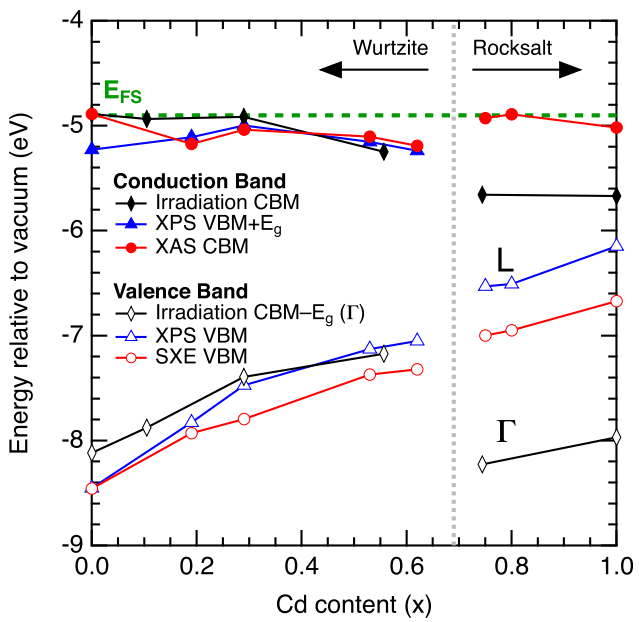

FIG. 6. The band edge shifts as measured by irradiation-induced Fermi-level pinning, XPS, and XAS/SXE, along with complementary band edge information that can be inferred by incorporating the intrinsic direct bandgap E_g from Ref. 11. All three techniques reveal that the narrowing of the intrinsic gap across the WZ composition range can be largely attributed to a >1 eV rise in the valence band. The indirect gap at the L-point observed in CdO is preserved for RS alloys.

Γ-point valence band position revealed by Fermi-level pinning and subsequent optical bandgap subtraction is complementary to the band edge extremum measured by the two X-ray spectroscopic techniques. Conversely, adding E_g to the VBM measured by XPS yields a value for the CBM, but only for direct-gap, WZ films.

There is good agreement among the three techniques about the observed changes in the band edges with composition. In the WZ-phase regime, there is excellent agreement between the directly measured (irradiation-CBM and XPS-VBM) and indirectly inferred (irradiation-VBM and XPS-CBM) band edges. The relative shifts observed by XAS/SXE support the conclusion that the considerable narrowing of the optical gap from 3.3 eV to 1.7 eV across the WZ composition range can be ascribed to the >1 eV shift of the VBM toward the vacuum level. For both RS samples, the VBM measured by XPS and XAS is considerably higher in energy than the Γ-point VBM inferred from irradiation, offering another indication that the indirect gap of the endpoint CdO is maintained for RS-alloys. Additionally, the ∼220 meV decrease in the Γ-point VBM for the RS alloy relative to that of the endpoint CdO partially accounts for the ∼300 meV difference in E_g we previously reported.[11]

Several previous studies have explored the electronic structure of the endpoint binary compounds,[22,24,25] with the natural band alignment calculated by Zhu *et al.* showing offsets in both the conduction band minima and valence band maxima of CdO and ZnO equilibrium phase structures.[25] In pure CdO, the valence band structure that gives rise to this L-point maximum is attributed to the proximity of shallow, filled Cd d levels to the VBM.[22]

The electronic structure of ternary $Cd_xZn_{1-x}O$ alloys was calculated by Schleife *et al.*,[13] indicating a total offset in the CBM ΔE_{CBM} of WZ alloys (that is, from x = 0 to the extrapolated value of WZ-CdO at x = 1) of ∼1 eV. The remaining band edge movement that contributes to the total narrowing of E_g (1.6 eV from x = 0 to x = 0.69) is predicted to come from the upward movement in the VBM. The magnitude of ΔE_{CBM} measured here for the WZ structured alloys is slightly less, approximately ∼600 meV across the full composition range, and contributes ∼400 meV to the total reduction in E_g. Each of the spectroscopic measurements in this study independently confirms that the upward rise in the VBM (>1 eV) is the origin of this bandgap tunability.

The nearly constant value of the CBM in the WZ and RS phase observed here explains the unusually weak composition dependence of the electron mobility we observed previously,[11] where the electron mobility of WZ alloys increases slightly from ∼15 $cm^2\ V^{-1}\ s^{-1}$ to ∼30 $cm^2\ V^{-1}\ s^{-1}$ over $0 < x < 0.69$. Typically, alloying of semiconductor materials results in a significant reduction of charge carrier mobilities by alloy disorder scattering. The strength of this scattering mechanism is related to the fluctuations of the CBM due to random atom distribution and is determined by ΔE_{CBM} for each phase regime. The mobility limit for alloy disorder scattering as a function of alloy composition x is

$$\mu_{AD} \propto \frac{1}{|\Delta E_{CBM}|^2 x(1-x)}, \tag{3}$$

following Ref. 26. As seen in Fig. 6, the values of ΔE_{CBM} measured by all three techniques for both WZ and RS phase are small, indicating that there is a negligible contribution from alloy disorder scattering.

Despite the relatively high electron concentration ($n \sim 10^{19}$ cm^{-3} to $n \sim 10^{20}$ cm^{-3}) of the as-grown samples, there is no distinguishable signal in the XPS spectra from filled states at the Fermi level. Even in the sample with the highest measured electron concentration, the RS alloy with $x = 0.74$ and $n \sim 2 \times 10^{20}$ cm^{-3}, this concentration corresponds to a native donor concentration of $<1\%$, near the detection limits of technique. Nonetheless, such a feature has been observed in the case of other nominally undoped transparent conducting oxides, such as In_2O_3.[27] The surface quality of the films in this study, as evidenced by the intensity of the O 1s peaks due to surface contamination, may help explain the absence of this feature.

The natural band alignments of $Cd_xZn_{1-x}O$ alloys are suggested by the average changes in the energies of the CBM and VBM presented in Figure 6. The locations of the band edges of several standard semiconductors can be directly inferred, given that the alignment of the endpoint compounds is already known. The proximity of the CBM of WZ-structured alloys to the VBM of some semiconductors (Si, Ge) suggests that CdZnO films may be attractive candidates for tandem photoelectrochemical (PEC) water splitting devices. In an n-Si/p-Si/WZ-CdZnO/RS-CdZnO device structure, the band alignments determined here suggest that it should be readily possible to form Ohmic contacts between naturally n-type WZ-CdZnO and p-type Si. Furthermore, the monotonic, upward rise in the VBM with Cd content across the entire $Cd_xZn_{1-x}O$ alloy system suggests that holes generated in linearly graded WZ-CdZnO absorbers would be swept into a top layer of RS-CdZnO, which in theory has several qualities of a good photoanode. The VBM of most oxides is positioned far too low relative to the oxidation potential of water to act as a viable photoanode to supply photogenerated holes to the oxygen evolution half reaction necessary for water splitting. The high VBM of CdO and RS-CdZnO makes them attractive candidates for this purpose. The low CBM, below the complementary reduction potential for hydrogen evolution, may limit photo-induced surface degradation at the water/device interface. Finally, the indirect gap of RS-CdZnO may provide yet another advantage for PEC applications: holes transferred into this layer will move to the L-point maximum and avoid immediate recombination.

VII. CONCLUSION

We have determined the band alignments of $Cd_xZn_{1-x}O$ alloys across the full composition range, finding good agreement among three independent measurements of VBM and CBM movement in order to explain optical trends such as the reduction in the intrinsic bandgap of luminescent WZ-CdZnO alloys, and the widening of the bandgap of RS-CdZnO alloys relative to CdO. The relatively stationary position of the CBM across the WZ composition range, and the correspondingly negligible role of alloy disorder scattering, explain the trends in the electron mobility reported previously. The rise in the VBM is larger than previously expected, and opens up opportunities for creating novel PEC device designs.

ACKNOWLEDGMENTS

This work, carried out at LBNL in the Materials Sciences Division and at the Advanced Light Source, was supported by the Director, Office of Science, Office of Basic Energy Sciences, of the U.S. Department of Energy under Contract No. DE-AC02-05CH11231. The authors would like to thank Jeffrey Beeman for his help with irradiation experiments and Alexander Luce for his help with XAS/SXE experiments.

[1]T. Makino, Y. Segawa, M. Kawasaki, A. Ohtomo, R. Shiroki, K. Tamura, T. Yasuda, and H. Koinuma, Appl. Phys. Lett. **78**, 1237 (2001).
[2]T. Gruber, C. Kirchner, R. Kling, F. Reuss, A. Waag, F. Bertram, D. Forster, J. Christen, and M. Schreck, Appl. Phys. Lett. **83**, 3290 (2003).
[3]S. Sadofev, S. Blumstengel, J. Cui, J. Puls, S. Rogaschewski, P. Schäfer, and F. Henneberger, Appl. Phys. Lett. **89**, 201907 (2006).
[4]J. Ishihara, A. Nakamura, S. Shigemori, T. Aoki, and J. Temmyo, Appl. Phys. Lett. **89**, 091914 (2006).
[5]X. J. Wang, I. A. Buyanova, W. M. Chen, M. Izadifard, S. Rawal, D. P. Norton, S. J. Pearton, A. Osinsky, J. W. Dong, and A. Dabiran, Appl. Phys. Lett. **89**, 151909 (2006).
[6]X. Ma, P. Chen, R. Zhang, and D. Yang, J. Alloys Compd. **509**, 6599 (2011).
[7]V. Venkatachalapathy, A. Galeckas, R. Sellappan, D. Chakarov, and A. Y. Kuznetsov, J. Cryst. Growth **315**, 301 (2011).
[8]S. Chu and G. Wang, Mater. Lett. **85**, 149 (2012).
[9]Y. Tian, X. Ma, L. Jin, D. Li, and D. Yang, Appl. Phys. Lett. **100**, 231101 (2012).
[10]H. H.-C. Lai, V. L. Kuznetsov, R. G. Egdell, and P. P. Edwards, Appl. Phys. Lett. **100**, 072106 (2012).
[11]D. M. Detert, S. H. N. Lim, K. Tom, A. V. Luce, A. Anders, O. D. Dubon, K. M. Yu, and W. Walukiewicz, Appl. Phys. Lett. **102**, 232103 (2013).
[12]X. D. Zhang, M. L. Guo, W. X. Li, and C. L. Liu, J. Appl. Phys. **103**, 063721 (2008).
[13]A. Schleife, C. Rödl, J. Furthmüller, and F. Bechstedt, New J. Phys. **13**, 085012 (2011).
[14]W. Walukiewicz, Phys. Rev. B **37**, 4760 (1988).
[15]W. Walukiewicz, Appl. Phys. Lett. **54**, 2094 (1989).
[16]E. O. Kane, J. Phys. Chem. Solids **1**, 249 (1957).
[17]S. X. Li, K. M. Yu, J. Wu, R. E. Jones, W. Walukiewicz, J. W. Ager III, W. Shan, E. E. Haller, H. Lu, and W. J. Schaff, Phys. Rev. B **71**, 161201 (2005).
[18]D. T. Speaks, M. A. Mayer, K. M. Yu, S. S. Mao, E. E. Haller, and W. Walukiewicz, J. Appl. Phys. **107**, 113706 (2010).
[19]M. A. Mayer, K. Yu, D. T. Speaks, J. Denlinger, L. A. Reichertz, J. W. Beeman, E. E. Haller, and W. Walukiewicz, J. Phys. Chem. C **116**, 15281 (2012).
[20]C. McGuinness, C. Stagarescu, P. Ryan, J. Downes, D. Fu, K. Smith, and R. Egdell, Phys. Rev. B **68**, 165104 (2003).
[21]I. N. Demchenko, M. Chernyshova, T. Tyliszczak, J. D. Denlinger, K. M. Yu, D. T. Speaks, O. Hemmers, W. Walukiewicz, G. Derkachov, and K. Lawniczak-Jablonska, J. Electron Spectrosc. **184**, 249 (2011).
[22]P. King, T. Veal, A. Schleife, J. Zúñiga-Pérez, B. Martel, P. Jefferson, F. Fuchs, V. Muñoz-Sanjosé, F. Bechstedt, and C. McConville, Phys. Rev. B **79**, 205205 (2009).
[23]W. Ma, Z. Ye, M. Lu, Y. Huang, H. Zhao, P. Zhu, J. Zhang, and M. He, Thin Solid Films **461**, 250 (2004).
[24]J. E. Jaffe, R. Pandey, and A. B. Kunz, Phys. Rev. B **43**, 14030 (1991).
[25]Y. Zhu, G. Chen, H. Ye, A. Walsh, C. Moon, and S.-H. Wei, Phys. Rev. B **77**, 245209 (2008).
[26]W. Walukiewicz, W. Shan, J. W. Ager III, D. R. Chamberlin, E. E. Haller, J. F. Geisz, D. J. Friedman, J. M. Olson, and S. R. Kurtz, in *Proceedings of the 195th Meeting* (Electro-Chem. Soc., 1999), Vol. 99–11, p. 190.
[27]A. Walsh *et al.*, Phys. Rev. Lett. **100**, 167402 (2008).